3. E. H. Hwang, S. Adam, S. Das Sarma, A. K. Geim, http://arXiv.org/abs/cond-mat/0610834.
4. C. Berger *et al.*, *Science* **312**, 1191 (2006); published online 12 April 2006 (10.1126/science.1125925).
5. Z. Chen, Y.-M. Lin, M. J. Rooks, P. Avouris, http://arXiv.org/abs/cond-mat/0701599.
6. M. Y. Han, B. Özyilmaz, Y. Zhang, P. Kim, http://arXiv.org/abs/cond-mat/0702511.
7. A. Rycerz, J. Tworzydło, C. W. J. Beenakker, *Nature Phys.* **3**, 172 (2007).
8. M. C. Lemme, T. J. Echtermeyer, M. Baus, H. Kurz, *IEEE Electron Device Lett.* **28**, 283 (2007).
9. B. Huard *et al.*, *Phys. Rev. Lett*. **98**, 236803 (2007).
10. K. S. Novoselov *et al.*, *Science* **306**, 666 (2004).
11. K. S. Novoselov *et al.*, *Nature* **438**, 197 (2005).
12. Y. Zhang, Y.-W. Tan, H. Stormer, P. Kim, *Nature* **438**, 201 (2005).
13. H. B. Heersche, P. Jarillo-Herrero, J. B. Oostinga, L. M. K. Vandersypen, A. F. Morpurgo, *Nature* **446**, 56 (2007).
14. M. I. Katsnelson, K. S. Novoselov, A. K. Geim, *Nature Phys.* **2**, 620 (2006).
15. V. V. Cheianov, V. I. Fal'ko, *Phys. Rev. B* **74**, 041403(R) (2006).
16. V. V. Cheianov, V. Fal'ko, B. L. Altshuler, *Science* **315**, 1252 (2007).
17. D. R. Smith, J. B. Pendry, M. C. K. Wiltshire, *Science* **305**, 788 (2004).
18. D. A. Abanin, L. S. Levitov, *Science* **317**, 641 (2007).
19. Information on materials and methods is available on *Science* Online.
20. D. B. Farmer, R. G. Gordon, *Nano Lett.* **6**, 699 (2006).
21. P. Gusynin, S. G. Sharapov, *Phys. Rev. Lett.* **95**, 146801 (2005).
22. A. Abanin, P. A. Lee, L. S. Levitov, *Phys. Rev. Lett.* **96**, 176803 (2006).
23. N. M. R. Peres, F. Guinea, A. H. Castro Neto, *Phys. Rev. B* **73**, 125411 (2006).
24. D. A. Syphers, P. J. Stiles, *Phys. Rev. B* **32**, 6620 (1985).
25. R. J. Haug, A. H. MacDonald, P. Streda, K. von Klitzing, *Phys. Rev. Lett.* **61**, 2797 (1988).
26. S. Washburn, A. B. Fowler, H. Schmid, D. Kern, *Phys. Rev. Lett.* **61**, 2801 (1988).
27. E. H. Hwang, S. Adam, S. Das Sarma, *Phys. Rev. Lett*. **98**, 186806 (2007); also available at http://arXiv.org/abs/cond-mat/0610157.

28. We thank L. S. Levitov, D. A. Abanin, C. H. Lewenkopf, and P. Jarillo-Herrero for useful discussions; Z. Chen at IBM T. J. Watson Research Center for suggesting the NO_2 functionalization process; and D. Monsma for assistance in implementing it. Research supported in part by INDEX and by the NSF through the Harvard Nanoscale Science and Engineering Center.

Supporting Online Material

www.sciencemag.org/cgi/content/full/1144657/DC1
Materials and Methods
SOM Text
Fig. S1

4 May 2007; accepted 15 June 2007
Published online 28 June 2007;
10.1126/science.1144657
Include this information when citing this paper.

Quantized Transport in Graphene *p-n* Junctions in a Magnetic Field

D. A. Abanin and L. S. Levitov*

Recent experimental work on locally gated graphene layers resulting in *p-n* junctions has revealed the quantum Hall effect in their transport behavior. We explain the observed conductance quantization, which is fractional in the bipolar regime and an integer in the unipolar regime, in terms of quantum Hall edge modes propagating along and across the *p-n* interface. In the bipolar regime, the electron and hole modes can mix at the *p-n* boundary, leading to current partition and quantized shot-noise plateaus similar to those of conductance, whereas in the unipolar regime transport is noiseless. These quantum Hall phenomena reflect the massless Dirac character of charge carriers in graphene, with particle/hole interplay manifest in mode mixing and noise in the bipolar regime.

The transport properties of graphene [two-dimensional sheets of graphite (*1*)], in particular the high carrier mobility and tunability of transport characteristics, make this material attractive for applications in nanoelectronics (*2*, *3*). Various methods have been developed for patterning graphene sheets into prototype devices such as quantum-dot transistors (*1*) and nanoribbons (*4*, *5*), followed by the demonstration of local control of carrier density in a graphene sheet (*6*). Besides possible device applications, graphene junctions are predicted to host new and exciting phenomena reflecting the massless Dirac character of carriers in this material, such as Klein tunneling (*7*), particle collimation (*8*), quasibound states (*9*), and Veselago lensing (*10*). In addition, interesting phenomena are expected in gated graphene bilayers, where field-effect transport can be induced by tuning the gap at the Dirac point (*11*). These applications make the gating of graphene a topic of great interest.

Recently, a graphene *p-n* junction with individual control of carrier density in two adjacent regions with a pair of gates above and below it was reported (*12*). The density in each region could be varied across the neutrality point, allowing *p-n*, *p-p*, and *n-n* junctions to be formed at the interface. The interface width was quite small, owing to the 30-nm distance to the top gate and its sharp edge. Transport measurements, carried out in the quantized Hall effect (QHE) regime at magnetic fields $3\ \mathrm{T} < B < 8\ \mathrm{T}$, revealed ohmic two-terminal conductance taking quantized values $g = 6, 2, 3/2$, and 1 in the units of conductance quantum e^2/h, where h is Planck's constant. The QHE plateaus with $g = 2$ and 6 were observed in the unipolar regime, whereas the quantized plateaus with $g = 1$ and $3/2$ of similar quality were observed in the bipolar regime. Whereas conductance of $6e^2/h$ and $2e^2/h$ is a hallmark of the integer QHE in graphene (*13*, *14*), quantized conductance values of $3/2$ and 1 are unusual and call for explanation.

We interpret these observations by linking them to the properties of the Dirac-like carriers, which give rise to bipolar electron and hole QHE edge modes at the *p-n* interface (Fig. 1). The behavior at the interface is explained by employing ideas from the theory of quantum-chaotic transport (*15*–*20*). Although in our case the edge modes carry charge along the *p-n* interface all in the same direction (in a chiral rather than chaotic fashion), we argue that intermode scattering within the *p-n* interface region gives rise to dynamics with features analogous to those known for quantum-chaotic systems.

In this analogy, the QHE states at the sample boundary play the role of perfect lead channels of chaotic quantum dots (*15*, *16*), bringing charge to the *p-n* interface and carrying it away into reservoirs. However, several physical effects causing conductance fluctuations in chaotic dots are absent in our case, leading to quantization of two-terminal conductance not known for the dots. In particular, the effective lead channels are quantized more perfectly than in the dots, owing to backscattering suppression in QHE transport. In addition, the quantum-mechanical interference effects, which lead to sample-specific conductance fluctuations, can be suppressed in our case because of self-averaging, as well as dephasing and electron-electron scattering. Other effects that can affect the edge-state transport at the *p-n* interface are

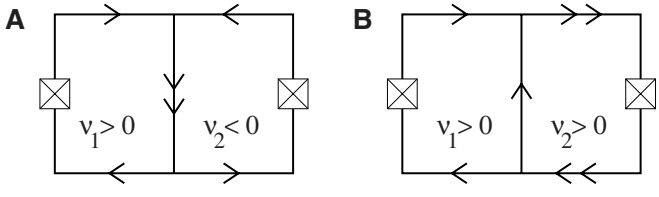

Fig. 1. Schematic of QHE edge states for the (**A**) bipolar regime and (**B**) unipolar regime of a graphene junction. In (A), the edge states counter-circulate in the *n* and *p* regions, bringing electrons and holes from different reservoirs to the *p-n* interface. Mode mixing at the interface leads to the two-terminal conductance (Eq. 1). In (B), because the edge states circulate in the same direction without backscattering or mixing, conductance is determined by the modes permeating the whole system, $g = \min(|\nu_1|, |\nu_2|)$.

Department of Physics, Center for Materials Sciences and Engineering, Massachusetts Institute of Technology, 77 Massachusetts Avenue, Cambridge, MA 02139, USA.

*To whom correspondence should be addressed. E-mail: levitov@mit.edu

intermode relaxation and coupling to electronic states in QHE bulk, causing dephasing in a manner similar to that of the voltage-probe model (*21*). Whereas these regimes yield similar results for conductance, they will manifest themselves differently in other characteristics, in particular in electron shot noise (*22*), which can be used for detailed characterization of transport mechanisms.

Because of particle/hole symmetry of carriers in graphene, the QHE in this material occurs symmetrically about the neutrality point at the densities $\nu = \pm 2, \pm 6, \pm 10...$ (*13*, *14*). In each of these quantized states, there are $n = |\nu|$ edge modes propagating in different directions at $\nu > 0$ and $\nu < 0$ (*23*, *24*). For the bipolar case, assuming QHE at densities $\nu_1 > 0$ and $\nu_2 < 0$ on either side of the boundary, this gives $|\nu_1|$ and $|\nu_2|$ edge modes circulating in opposite directions that merge to form a multimode edge state at the *p-n* interface (Fig. 1A). These modes supply to the *p-n* interface particles from both the *n* and *p* reservoirs. After propagating together along the interface, these particles arrive at the sample boundary where they are ejected into the edge modes, which split up and return to reservoirs.

The observed conductance quantization can be readily explained by assuming full mixing of these modes at the *p-n* interface, so that for each particle the probability to be ejected into any of the $N = |\nu_1| + |\nu_2|$ modes equals $p_N = 1/N$, irrespective of its origin. The two-terminal conductance is then obtained by multiplying p_N by the numbers of the modes, giving

$$g_{pn} = \frac{|\nu_1||\nu_2|}{|\nu_1| + |\nu_2|} = 1, \frac{3}{2}, 3, \frac{5}{3} \ldots \qquad (1)$$

where $\nu_{1,2} = \pm 2, \pm 6, \pm 10....$ This agrees with the observed quantized values (*12*) (Fig. 2).

The character of QHE edge transport in the unipolar regime is quite different. In this case, *n-n* or *p-p*, the edge modes in both regions circulate in the same direction. As a result, some modes are coupled to both reservoirs, whereas the others are connected to only one of the reservoirs (Fig. 1B). With backscattering suppressed by QHE, the conductance across the boundary is solely due to those edge modes that permeate the entire system, making contact with both reservoirs. This gives the observed nonclassical conductance values

$$g_{nn} = g_{pp} = \min(|\nu_1|,|\nu_2|) = 2, 6, 10... \qquad (2)$$

where $\nu_{1,2} = \pm 2, \pm 6, \pm 10...$, in agreement with the known results for the quantized conductance of constrictions between different QHE states (*25*, *26*). The nondissipative character of transport in the unipolar regime (Eq. 2), resulting from suppressed backscattering, can be revealed by measuring noise. In the absence of current partitioning inside the sample, we expect only thermal Johnson-Nyquist noise $S = 2gk_BT$ (where k_B is the Boltzmann constant and T is temperature) in this regime, but no shot-noise contribution (Fig. 3).

The conductance values given by Eqs. 2 and 1 occur in a particular pattern (*12*) that can be described as follows (Fig. 2): Electron density in graphene induced by the back gate is $n_1 = (\kappa/4\pi e)V_b/d$, where d is the distance to the gate, V_b is the voltage on it, and κ is the dielectric constant. Similarly, in the locally gated region we have $n_2 = (\kappa/4\pi e)(V_b/d + V_t/h)$, where h and V_t are the distance to the top gate and the voltage on it. For the Landau-level filling factors $\nu_{1,2} = (hc/eB)n_{1,2}$ we find

$$\nu_1 = (l_B^2\kappa/2e)V_b/d,$$
$$\nu_2 = (l_B^2\kappa/2e)(V_b/d + V_t/h) \qquad (3)$$

where l_B is the magnetic length. The values V_b and V_t, corresponding to integer QHE states, are inside parallelograms with the boundaries approximately given by $\nu_{1,2} = 0, \pm 4, \pm 8...$, as appropriate for the fourfold degenerate graphene Landau levels (*13*, *14*). The resulting conductance pattern, shown in Fig. 2 for realistic parameter values, strikingly resembles the experimental results (*12*).

How is the conductance in Eq. 1 affected by quantum-mechanical interference effects? Random-matrix theory (RMT) of chaotic transport predicts (*15*, *16*) ensemble-averaged conductance $\bar{g} = n_1n_2/(n_1 + n_2 + 1 - 2/\beta)$, where $n_{1,2}$ is the open channel number and $\beta = 1$, 2, or 4 for the three random-matrix universality classes. In our QHE case, with the channel numbers $n_{1,2} = |\nu_{1,2}|$ and $\beta = 2$, RMT predicts that $\bar{g}$ is identical to Eq. 1. Similarly, a semiclassical description of transport in chaotic cavities (*17*), where mixing is due to the dynamics in the cavity, yields conductance values close to the classical result for two conductors connected in series.

To clarify the origin of the mode mixing at the *p-n* interface, we studied electron-density distribution for the gate geometry used in (*12*). A numerical solution of the Laplace problem for the electrostatic potential in between the gates revealed that the *p-n* density step is about 40 nm wide, a few times larger than the magnetic length at $B = 8$ T. Comparison to the known results (*27*) for a compressible region sandwiched between incompressible regions then suggests the presence at the *p-n* interface of additional QHE

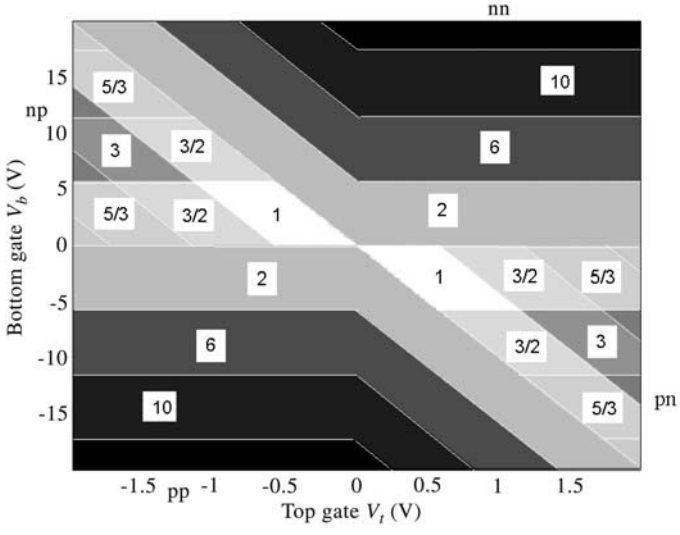

Fig. 2. Two-terminal conductance versus gate voltage, given by Eq. 1 in the bipolar case ($\nu_1 > 0$, $\nu_2 < 0$) and by Eq. 2 in the unipolar case ($\nu_{1,2}$ of equal sign). The boundaries of QHE regions are specified by $\nu_{1,2} = 0, \pm 4, \pm 8...$, with the gate voltage dependence of $\nu_{1,2}$ given by Eq. 3. The parameters used are as follows: distance to the top gate $h = 30$ nm, distance to the back gate $d = 300$ nm, magnetic length $l_B = 10$ nm, and dielectric constant $\kappa = 3$.

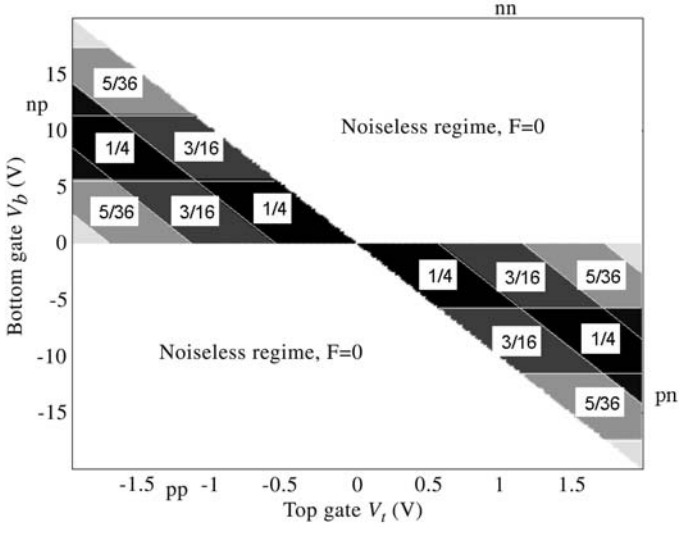

Fig. 3. Shot-noise Fano factor (Eq. 8) plotted versus gate voltages for the same parameter values as those in Fig. 2. The noise is zero in the unipolar regime (*p-p* or *n-n*), reflecting the absence of QHE edge-state backscattering and current partition at the junction interface. In the bipolar regime, because of edge mode mixing at the *p-n* interface, noise is finite, exhibiting a quantized plateau structure similar to that of conductance.

modes which, in the presence of disorder, can facilitate interchannel scattering and mixing.

In the fully coherent regime, conductance would exhibit universal fluctuations (UCF). The magnitude of UCF predicted for chaotic transport (*20*) in our case depends on the channel numbers as follows

$$\mathrm{var}(g) = \frac{\nu_1^2\nu_2^2}{(|\nu_1|+|\nu_2|)^2[(|\nu_1|+|\nu_2|)^2-1]} \quad (4)$$

Applied to the observed plateaus with $(\nu_1,\nu_2) = (2,-2)$, $(2,-6)$, and $(6,-2)$, Eq. 4 indicates that these plateaus would not have been discernible in a system with fully developed UCF. We therefore conclude that the observed quantization of g depends on some mechanism that suppresses UCF. For example, the suppression could easily be understood if Thouless energy for the states at the *p-n* interface was small as compared with k_BT. The reduced UCF would then result from averaging over the k_BT energy interval. However, the plateaus in (*12*) remain unchanged when the temperature is reduced from 4 K to 250 mK, making such a scenario unlikely.

The UCF suppression may signal a fundamental departure of chiral QHE dynamics from that of the earlier-studied systems. However, at this point we cannot exclude other, more mundane explanations. In particular, time-dependent fluctuations of system parameters can supercede mesoscopic fluctuations, turning the observed time-averaged quantities into ensemble-averaged quantities. This self-averaging could arise naturally because of a fluctuating electric field at the *p-n* interface induced by voltage noise on the gates. Another, more interesting explanation could be that UCF suppression indicates the presence of dephasing due to the coupling of the chiral modes to the localized states in the bulk, or some other intrinsic mechanism.

Current partition because of mode mixing at the *p-n* interface will manifest itself in the finite shot-noise intensity. To find noise, we take into account that the mixing of the reservoir distributions, no matter of what origin, results in particle energy distribution of a double-step form

$$n(\varepsilon) = \frac{|\nu_1|}{N}n_1(\varepsilon) + \frac{|\nu_2|}{N}n_2(\varepsilon) \quad (5)$$

where $n_{1,2}(\varepsilon) = n_F(\varepsilon \pm \frac{1}{2}V_{sd})$. [Here, $n_F(\varepsilon)$ is the Fermi distribution, and V_{sd} is the source-drain voltage.] In an analogy with diffusive systems (*28*) and chaotic cavities (*17*, *19*), this distribution serves as a Kogan-Shulman–like extraneous source of current fluctuations

$$J = \int n(\varepsilon)[1-n(\varepsilon)]d\varepsilon = \frac{|\nu_1||\nu_2|}{N^2}|V_{sd}| \quad (6)$$

We relate the noise source J to the fluctuations of the two-terminal current by noting that, because fluctuating current of intensity J is injected into each open channel, the current fluctuations flowing into the n and p regions will be $J_1 = |\nu_1|J$ and $J_2 = |\nu_2|J$. Converting these fluctuations into voltage fluctuations and adding the contributions of the n and p regions, we find the voltage fluctuations δV induced between the reservoirs

$$\langle \delta V^2 \rangle = \frac{J_1}{|\nu_1|^2} + \frac{J_2}{|\nu_2|^2} = \left(\frac{1}{|\nu_1|}+\frac{1}{|\nu_2|}\right)J = \frac{|V_{sd}|}{N} \quad (7)$$

Current noise can now be obtained as $S = g^2\langle \delta V^2 \rangle$, where g is the conductance (Eq. 1). It is convenient to characterize noise by the Fano factor $F = S/I$ (where I is current), describing noise suppression relative to Poisson noise. We find

$$F = \frac{|\nu_1||\nu_2|}{(|\nu_1|+|\nu_2|)^2} = \frac{1}{4}, \frac{3}{16}, \frac{5}{36}\ldots \quad (8)$$

where $\nu_{1,2} = 2, 6, 10....$ The result (Eq. 8) is identical in form to the shot-noise Fano factors of chaotic cavities (*17*, *19*). The Fano factor values (Eq. 8) should be contrasted with $F \approx 0.29$ that is predicted for a *p-n* junction in the absence of magnetic field (*8*).

Another regime for noise is possible if electrons, while traveling along the *p-n* interface, have enough time to transfer energy to each other via inelastic processes. This will occur if $\tau_{el} \ll L/v$, where τ_{el} is the characteristic electron energy relaxation time, v is the drift velocity, and L is the *p-n* interface length. [A similar regime was analyzed for diffusive (*28*) and chaotic (*19*) transport.] In this case, the electron energy distribution is characterized by an effective temperature T_{eff} that is determined by the balance of the energy supplied from reservoirs and electron thermal energy flowing out

$$\frac{1}{2}\frac{|\nu_1||\nu_2|}{|\nu_1|+|\nu_2|}V_{sd}^2 = \frac{\pi^2}{6}(|\nu_1|+|\nu_2|)k_B^2T_{eff}^2 \quad (9)$$

The extraneous fluctuations (Eq. 6), evaluated for the Fermi distribution with $T = T_{eff}$, give $J = k_BT_{eff}$. Repeating the reasoning that has led to Eq. 8, we find the noise intensity $S = gk_BT_{eff}$. This expression resembles the Nyquist formula, except for the factor of 2 missing because the fluctuations (Eq. 6) occur only in the *p-n* region but not in the leads. Because $T_{eff} \propto V_{sd}$, this noise is linear in V_{sd}. Similar to the $T = 0$ shot noise, it can be characterized by the Fano factor $\tilde{F} = (3F)^{1/2}/\pi$, with F given by Eq. 8.

Finally, noise can be used to test which of the UCF suppression mechanisms discussed above, self-averaging or dephasing, occurs in an experiment (*12*). For coherent transport, noise exhibits mesoscopic fluctuations, similar to UCF, that can be analyzed within an RMT framework. In the absence of time-reversal symmetry, RMT yields an ensemble-averaged Fano factor

$$\overline{F} = \frac{|\nu_1||\nu_2|}{(|\nu_1|+|\nu_2|+1)(|\nu_1|+|\nu_2|-1)} \quad (10)$$

[see Eq. 11 in (*20*)]. For $\nu_{1,2} = 2, 4, 6...$, this gives $\overline{F} = 4/15, 12/63, 36/143....$ These values, expected when transport is coherent but self-averaged, are different from those in Eq. 8 that are obtained from an incoherent-mixing model.

The quantized transport observed in graphene *p-n* junctions (*12*) is of different character in the unipolar and bipolar regimes. In the first case, transport is dissipationless, with conductance quantized to an integer. In the second case, mode mixing at the *p-n* interface creates a situation similar to that studied in quantum-chaotic transport. Conductance quantized to fractional values observed in (*12*) then results from intrinsic or extrinsic suppression of UCF. These transport regimes can be unraveled by using electron shot noise (predicted to be finite in the bipolar regime and zero in the unipolar regime), with quantized plateau structure similar to that of conductance.

References and Notes

1. A. K. Geim, K. S. Novoselov, *Nat. Mater.* **6**, 183 (2007).
2. Y.-W. Son, M. L. Cohen, S. G. Louie, *Nature* **444**, 347 (2006).
3. A. Rycerz, K. J. Tworzydlo, C. W. J. Beenakker, *Nat. Phys.* **3**, 172 (2007).
4. Z. Chen, Y.-M. Lin, M. J. Rooks, P. Avouris, preprint available at http://arXiv.org/abs/cond-mat/0701599.
5. M. Y. Han, B. Oezyilmaz, Y. Zhang, P. Kim, preprint available at http://arXiv.org/abs/cond-mat/0702511.
6. B. Huard *et al.*, preprint available at http://arXiv.org/abs/0704.2626.
7. M. I. Katsnelson, K. S. Novoselov, A. K. Geim, *Nat. Phys.* **2**, 620 (2006).
8. V. V. Cheianov, V. I. Fal'ko, *Phys. Rev. B* **74**, 041403 (2006).
9. P. G. Silvestrov, K. B. Efetov, *Phys. Rev. Lett.* **98**, 016802 (2007).
10. V. V. Cheianov, V. Fal'ko, B. L. Altshuler, *Science* **315**, 1252 (2007).
11. T. Ohta, A. Bostwick, T. Seyller, K. Horn, E. Rotenberg, *Science* **313**, 951 (2006).
12. J. R. Williams, L. DiCarlo, C. M. Marcus, *Science* **317**, 638 (2007).
13. K. S. Novoselov *et al.*, *Nature* **438**, 197 (2005).
14. Y. Zhang, Y.-W. Tan, H. L. Stormer, P. Kim, *Nature* **438**, 201 (2005).
15. C. W. J. Beenakker, *Rev. Mod. Phys.* **69**, 731 (1997).
16. H. U. Baranger, P. A. Mello, *Phys. Rev. Lett.* **73**, 142 (1994).
17. Ya. M. Blanter, E. V. Sukhorukov, *Phys. Rev. Lett.* **84**, 1280 (2000).
18. O. Agam, I. Aleiner, A. I. Larkin, *Phys. Rev. Lett.* **85**, 3153 (2000).
19. S. Oberholzer *et al.*, *Phys. Rev. Lett.* **86**, 2114 (2001).
20. D. V. Savin, H.-J. Sommers, *Phys. Rev. B* **73**, 081307(R) (2006).
21. M. Büttiker, *Phys. Rev. B* **38**, 9375 (1988).
22. Ya. M. Blanter, M. Büttiker, *Phys. Rep.* **336**, 1 (2000).
23. N. M. R. Peres, F. Guinea, A. H. Castro Neto, *Phys. Rev. B* **73**, 125411 (2006).
24. D. A. Abanin, P. A. Lee, L. S. Levitov, *Phys. Rev. Lett.* **96**, 176803 (2006).
25. R. J. Haug, A. H. MacDonald, P. Streda, K. von Klitzing, *Phys. Rev. Lett.* **61**, 2797 (1988).
26. S. Washburn, A. B. Fowler, H. Schmid, D. Kern, *Phys. Rev. Lett.* **61**, 2801 (1988).
27. A. V. Khaetskii, V. I. Fal'ko, G. E. W. Bauer, *Phys. Rev. B* **50**, 4571 (1994).
28. K. E. Nagaev, *Phys. Lett. A* **169**, 103 (1992).

29. We thank C. M. Marcus, L. DiCarlo, J. R. Williams, P. Kim, and P. Jarillo-Herrero for discussions and Ya. M. Blanter and E. V. Sukhorukov for comments. This work is supported by the NSF Materials Research Science and Engineering Center (grant DMR-02132802) and NSF (grant DMR-0304019).

4 May 2007; accepted 21 June 2007
Published online 28 June 2007;
10.1126/science.1144672
Include this information when citing this paper.